Journal of Environmental Chemical Engineering 9 (2021) 106671

Contents lists available at ScienceDirect

Journal of Environmental Chemical Engineering

journal homepage: www.elsevier.com/locate/jece

Development of a photocatalytic zirconia-titania ultrafiltration membrane with anti-fouling and self-cleaning properties

Fabrício Eduardo Bortot Coelho [a,*], Dennis Deemter [b], Victor M. Candelario [c], Vittorio Boffa [d], Sixto Malato [b], Giuliana Magnacca [a]

[a] Department of Chemistry, University of Turin, Via P. Giuria 7, 10125 Torino, Italy
[b] Plataforma Solar de Almería-CIEMAT, Carretera de Senés Km 4, Tabernas, Almería, Spain
[c] Department of Research and Development, Liqtech Ceramics A/S, Industriparken 22 C, 2750 Ballerup, Denmark
[d] Department of Chemistry and Bioscience, Aalborg University, Fredrik Bajers Vej 7H, DK-9220 Aalborg Øst, Denmark

ARTICLE INFO

Keywords:
Anti-fouling
Photocatalytic membranes
Water treatment
Silicon carbide
Ceramic membranes

ABSTRACT

A photocatalytic Ce-Y-ZrO_2/TiO_2 ultrafiltration membrane was successfully prepared on a ZrO_2/SiC support by a modified sol-gel process. The top active layer is 2 μm thick, uniform and defect-free. The membrane presented a molecular weight cut-off (MWCO) of 19 kDa (equivalent to a pore size of 6 nm) and a high pure water permeability, 160 $Lm^{-2}h^{-1}bar^{-1}$. The high hydrophilicity and negative surface charge of the membrane favoured its great retention of proteins (bovine serum albumin, whey protein, and hemoglobin), indigo dye, and humic acid. The membrane was effective in photodegrading phenol and humic acid under simulated sun light irradiation. During humic acid filtration tests, the membrane presented better anti-fouling properties (smaller flux decline) and higher permeate flux under irradiation compared to the filtration in the dark. Moreover, self-cleaning properties were observed by irradiating the membrane, which enabled recovering up to 97% of the original flux. Consequently, a longer operation without chemical cleaning is possible, reducing costs and the process footprint. Further investigation would allow the development of innovative treatments for dinking and wastewaters by combining filtration and advanced oxidation processes for the abatement of contaminants of emerging concern in the presence of natural organic matter.

1. Introduction

Water is the most precious resource in the world. It is essential in every aspects of life and economy [1]. A global water crisis is on course since water demand and pollution keep increasing while many people still do not have supply of clean water [2]. All these aggravated by the uncertainties of climate change [3]. Therefore, the world urges for sustainable, cost-effective, and reliable methods for drinking water purification and wastewater treatment [4,5]. Compared to traditional technologies, membrane filtration has many advantages such as high quality permeate, little or no chemicals requirement, ease of operation, and modular construction, allowing its easy upscale [6,7]. Polymeric membranes have been dominant in water treatment [8] but their poor long-term stability limits their application [1]. On the other hand, ceramic membranes have extreme thermal, mechanical, and chemical resistance, longer lifetimes, higher hydrophilicity, high fluxes at low pressures, higher porosity, and lower fouling compared to polymeric membranes [8,9]. Therefore, ceramic membranes are suitable for challenging water purification processes [10] and harsh environments [11] to be applied, for instance, to textile and pharmaceutical wastewater treatment, humic-rich surface water purification [12], oil/water separation, mining, and food and beverage industry [13].

Nevertheless, ceramic membranes also have some drawbacks, such as high temperature sintering and the challenges in obtaining micropores [14]. At the same time, membrane fouling still one of the most critical issues in the development of membrane processes, since it reduces the system performance, increases operation costs, and decelerates the scale-up to industrial applications [15]. Fouling is characterized by the reduction of the permeate flux or increase of the transmembrane pressure as a result of the blockage of the membrane pores [16]. The major causes of fouling are the adsorption of feed solutes, the deposition of particles, the gel formation, and the bacterial growth (bio fouling) [16]. In surface waters and wastewaters filtration, fouling is caused mainly by the presence of organic compounds [17],

* Corresponding author.
E-mail address: fabricioeduardo.bortotcoelho@unito.it (F.E. Bortot Coelho).

https://doi.org/10.1016/j.jece.2021.106671
Received 26 July 2021; Received in revised form 22 October 2021; Accepted 23 October 2021
Available online 28 October 2021

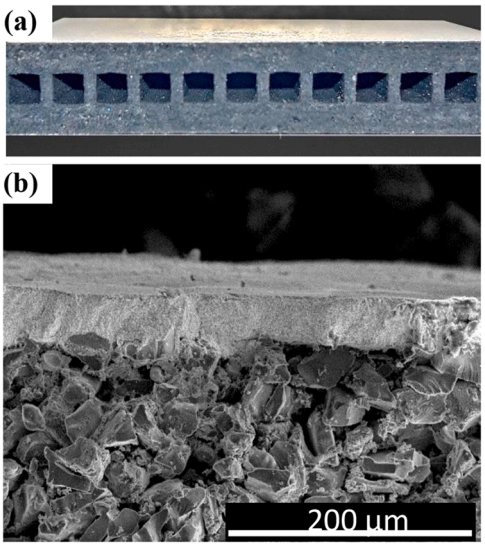

Fig. 1. (a) ZrO_2/SiC support and its (b) cross-section SEM image.

which can be dyes, surfactants, oil, and phenolic compounds [13,18], or natural organic matter (NOM), such as humic and fulvic acids [17,19]. When the dissolved matter is adsorbed onto the membrane surface and/or in the pores, it is considered an irreversible fouling [20], which usually requires chemical cleaning to recover the original flux [21] often shortening the lifetime of the membranes [9]. In this way, many strategies were developed for fouling prevention, some of them related to operation conditions (e.g. backwashing, pre-treatment of the feed, critical flux, and high cross flow velocity [22,23]), and others focused on the membrane modification, such as functionalization with polymers [24], nanoparticles [15], and catalysts [13,25].

Recently, great achievements have been reported for catalytic ceramic membranes with not only anti-fouling and self-cleaning properties [26–29] but also serving additional functions, such as disinfection [27] and pollutant degradation [30]. These membranes combine filtration with Advanced Oxidation Processes (AOP), in which reactive oxygen species (ROS), such as hydroxyl radicals ($^{\bullet}OH$), are generated to degrade organic pollutants into inorganic molecules [31]. There are many ways to generate ROS, for instance photocatalysis, in which light is absorbed by a semiconductor catalyst generating photoinduced holes and electrons that react with water and dissolved oxygen [22], or Fenton processes, where the a catalytic decomposition of the oxidant, hydrogen peroxide (H_2O_2) in presence of Fe^{2+}, generates $^{\bullet}OH$ radicals [32]. In the photo-Fenton process, the organics degradation is enhanced by light irradiation, which promotes the catalyst regeneration by the photo-reduction of Fe^{3+} to Fe^{2+} [32]. Another approach is to use photocatalysis to generate H_2O_2 and promote the Fenton reaction by adding Fe^{2+} to the system [33].

Mendret et al. [28], observed that UV irradiation prevented flux decline in the filtration of the dye Acid Orange 7 with their photocatalytic TiO_2/Al_2O_3 membrane (pore size below 0.2 µm) prepared by a sol-gel route. However, in their work and in many others reported in the literature [30,34,35], the photocatalytic layer is not an efficient separation layer because it is not homogeneous or because the catalyst particles were only stably immobilized on the membrane. This is explained by the challenges faced in fabricating a defect-free separation layer with small pore size without losing the catalytic activity [36]. Even though, several authors were able to fabricate ceramic membranes in which the top layer actually acts as photocatalytic and separation layer [18,26–29,37]. For instance, Manjumol et al. [36] developed an Al-TiO_2 ultrafiltration membrane with a pore size around 11 nm able to separate and degrade methylene blue under UV-light irradiation. In their study and in the majority of the reports, the active layer is deposited on macro/mesoporous alumina supports [18,26–30,34–37], but they suffer insufficient chemical and thermal stability to operate under corrosive and aggressive conditions such as very low or high pH [38,39].

Therefore, in the present work, an ultrastable macroporous silicon

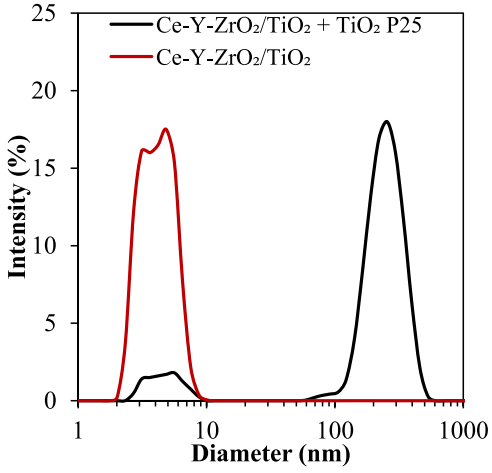

Fig. 3. Particle size distribution of the Ce-Y-ZrO_2/TiO_2 sol and the coating fluid, Ce-Y-ZrO_2/TiO_2 + TiO_2 P25, measured by DLS.

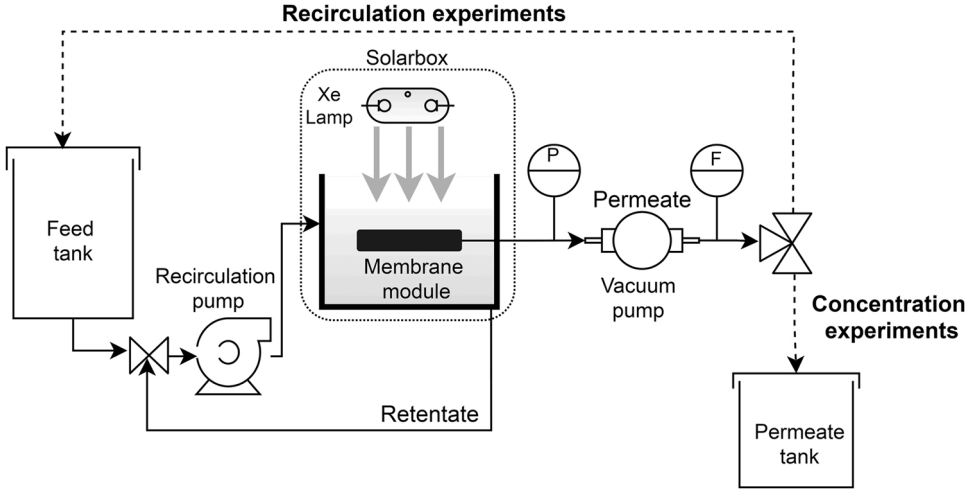

Fig. 2. Scheme of the experimental filtration set-up.

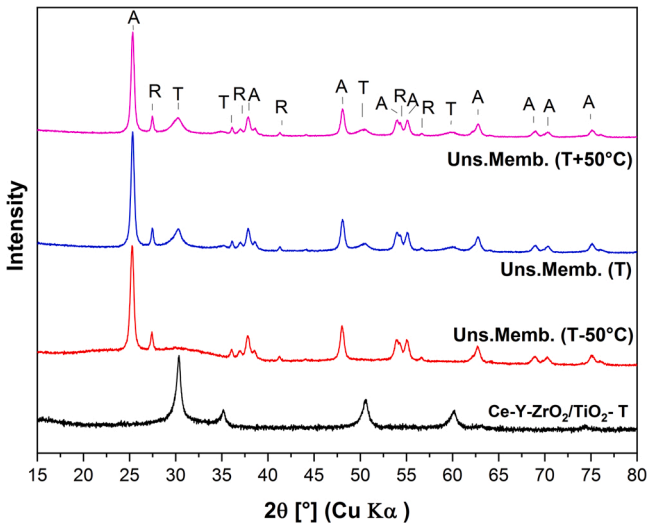

Fig. 4. X-ray diffactograms of the Ce-Y-ZrO_2/TiO_2 gel fired at temperature T and unsupported membranes fired at different temperatures. A=anatase TiO_2, R=rutile TiO_2, T = tetragonal ZrO_2.

carbide (SiC) support with a mesopouros zirconia (ZrO_2) intermediate layer was chosen as a matrix for preparing a photocatalytic membrane by a sol-gel technique. Both SiC and ZrO_2 are refractory materials that can work at high temperatures [14], they also possess high mechanical strength and chemical resistance [40–42], which make them applicable in harsh environments, highly contaminated feeds, acid and basic media [38], where other materials fail [43,44]. In addition, the very good mechanical properties of these materials able them in supporting high pressures, backwashing, aggressive cleaning and disinfection processes [45].

To the best of our knowledge, there is no preceding study that has specifically explored the fabrication of photocatalytic membranes on a SiC support. In the present work, a mixed oxide was used as catalyst, namely cerium-doped zirconia (Ce-ZrO_2) in combination with titanium dioxide (TiO_2). TiO_2 is the most studied and widely applied photocatalyst [31,34,46], but there is a limitation to practical application of pure titania membranes due to the reduction of porosity and cracks formation caused by the partial anatase to rutile phase transformation that occurs upon sintering at temperatures higher than 350 °C [35]. In addition, pure zirconia membranes can crack during sintering because of large volume variation (~4–9%) involved in the monoclinic to tetragonal phase transformation [14,38]. To overcome these drawbacks, a mixed TiO_2/ZrO_2 oxide was chosen as catalyst. In fact, it is known that in a Ti-doped zirconia, the tetragonal phase is partially stabilized and its crystallisation temperature increases up to 550 °C [47], which prevents crack formation and loss of porosity during membrane sintering [48], allowing the formation of a homogeneous separation layer with smaller pore size and higher catalytic activity than those exposed by the pure oxides [35,49,50]. Moreover, by adding cerium to zirconia, the resulting material partially absorbs visible light [51,52] and it is activated to generate reactive oxygen species, with a great potential to degrade organic compounds, or to oxidize directly the organic molecules [53] exploiting solar irradiation.

Another challenge in preparing small pore size membranes by sol-gel technique is the excessive infiltration of the sol particles into the support framework [54], which usually has elevated surface roughness, favouring cracks and pinholes in the membrane layer [55]. In order to solve this problem, TiO_2 P25 nanoparticles were added to the gel to prevent penetration of the sol allowing the formation of a homogeneous layer.

In this context, the aim of the present study was threefold. First, to investigate the deposition of a Ce-Y-ZrO_2/TiO_2 photocatalytic ultrafiltration membrane on a ZrO_2/SiC support, optimizing the coating and sintering conditions. Second, to characterize the membrane morphology, pore size, permeability, retention and photocatalytic activity towards phenol, a molecule that does not suffer direct photolysis [56], as model contaminant instead of the more classically used dyes [26,28,29,35,36]. Third, to evaluate the anti-fouling and self-cleaning properties of the developed membrane using humic acid (HA) as a model foulant.

2. Materials and methods

2.1. Membrane fabrication

2.1.1. Support materials

The membranes were coated on highly porous multi-channelled SiC flat sheet supports with a monoclinic ZrO_2 intermediate layer supplied by Liqtech Ceramics A/S (Denmark). Each support has 100 ± 1 mm of width, a total length of 150 ± 2 mm, and 25 channels of 2 × 2 mm each (Fig. 1a and b). The support and the intermediate layer have pore sizes of 15 μm and 60 nm, respectively, no cracks or pinholes, and a smooth surface. This support is made for submerged outside-in filtration, being able to operate in a pH range from 0 to 14 and temperatures up to 800 °C, according to the manufacturer.

2.1.2. Zr/Ti sols preparation and coating

A modified colloidal sol-gel process (Fig. S.1) was used to fabricate the photocatalytic ultrafiltration membrane. In a beaker, Ce $(NH_4)_2(NO_3)_6$ (CAS 16774–21–3, >98.5%, Aldrich) was dissolved in 2-propanol (CAS 67–63–0, >99.5%, Sigma-Aldrich). Next, titanium isopropoxide $Ti(OCH(CH_3)_2)_4$ (CAS 546–68–9, 97%, Sigma-Aldrich) and zirconium propoxide $Zr(OC_3H_7)_4$ (CAS 23519–77–9, 70%, Sigma-Aldrich) were added to mixture. The hydrolysis and peptization of these alcoxides were carried out with the addition of HNO_3 (CAS 7697–37–2, 65%, Sigma-Aldrich) under strong stirring. This system was brought to ebullition and kept under reflux until a completely transparent bluish sol was obtained. Yttrium nitrate ($Y(NO_3)_3.6\ H_2O$) (CAS 13494–98–9, 99.8%, Sigma-Aldrich) was then added to the sol. Part of this sol was dried and the resulting gel calcined for characterization. Next, AEROXIDE® TiO_2 P25 powder (Evonik, Germany) was dispersed into this sol by ultrasonication. A temporary binder, based on polyvinyl alcohol (PVA), was added to adjust the coating fluid viscosity, control the infiltration of the coating into the support, and increase the strength of the green body (membrane layer before sintering). Unsupported membranes were obtained by the dried coating fluid after calcination at different temperatures (400 <T < 700 °C).

The Ce-Y-ZrO_2/TiO_2 top layer was fabricated by dip coating the ZrO_2/SiC supports into the coating fluid for a determined interval of time. The green membrane was dried overnight at room temperature

Table 1
Phase composition, crystallite size, and band gap (E_g) of the unsupported membrane (Ce-Y-ZrO_2/TiO_2 +TiO_2 P25) fired at different temperatures.

Firing temperature (°C)	ZrO_2	TiO_2		Anatase:Rutile	Crystallite size (nm)		Eg (eV)
	Tetragonal (wt%)	Anatase (wt%)	Rutile (wt%)		t-ZrO_2	a-TiO_2	
T-50	Amorphous	88	12	7:1	–	33	–
T	18	72	10	7:1	7.0	40	2.5 / 3.1
T + 50	18	72	10	7:1	7.3	48	2.4 / 3.0

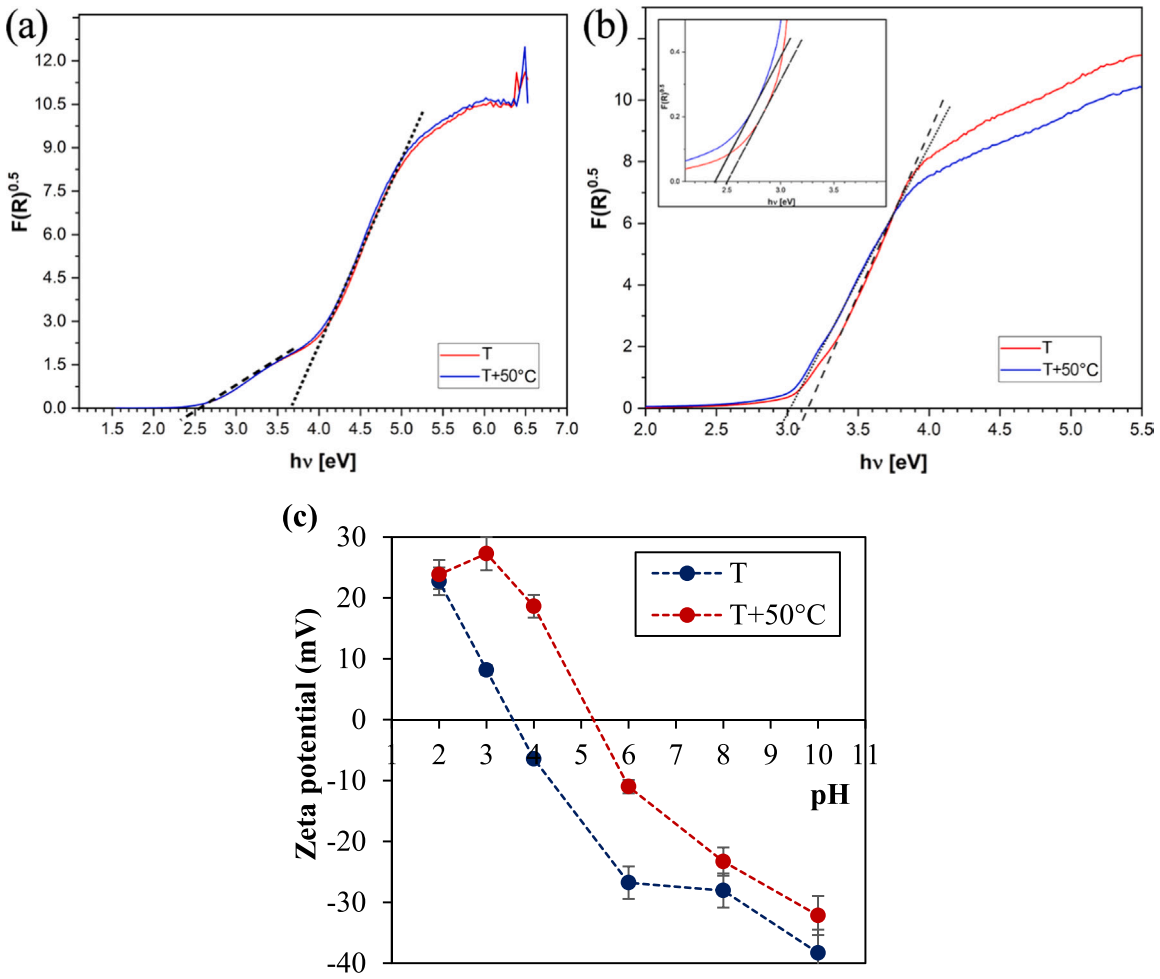

Fig. 5. Tauc's plot ($F(R)^{0.5}$) for the UV–vis diffuse reflectance spectroscopy of the fired (a) Ce-Y-ZrO_2/TiO_2 gels and (b) unsupported membranes. (c) Zeta potential of the unsupported membranes fired at different temperatures.

and kept 1 h in a drying cabinet at 40 °C. A second dip coating and drying cycle was performed, and the green membranes were sintered in air in three different temperatures with a heating rate of 1 °C min^{-1}, in order to minimize the crack formation. Own to confidentiality issues, the three different sintering temperatures were reported as T-50, T, T + 50 °C, with T in the range between 400 and 700 °C.

The obtained sol, fired gel, coating fluid, and unsupported membrane were characterized in terms of phase composition, particle size, zeta potential and UV-Vis absorption. X-rays diffraction (XRD) patterns were obtained with a diffractometer PW3040/60 X'Pert PRO MPD (Malvern Panalytical, Netherlands), operating at 45 kV, 40 mA, with a Cu Kα radiation source (λ = 1.5418 Å) and a Bragg Brentano geometry over the range $10° < 2\theta < 80°$. Particle size analysis and zeta potential measurements were performed on a Zetasizer Nano ZS (Malvern Panalytical, Netherlands) using principles of laser Doppler velocitometry and phase analysis light scattering (M3-PALS technique). 0.1% *w/v* suspensions were prepared, their pH adjusted with HCl or NaOH solution, and then ultrasonicated for 10 min before the analysis. Diffuse Reflectance Spectroscopy (DRS) data were recorded in the 200–800 nm range using a Cary 5000 spectrometer (Agilent, CA, USA), coupled with an integration sphere for diffuse reflectance studies, using a Cary win-UV/scan software. A sample of PTFE with 100% reflectance was used as the reference. The optical band gap energy has been calculated from the Tauc plot.

2.2. Membrane characterization

The morphology of the developed membranes was analysed by Scanning electron microscopy (SEM) using a microscope EVO 50 XVP (ZEISS, Germany) with a LaB_6 source, equipped with detectors for backscattered electrons, secondary electrons collection, and energy dispersive X-ray Spectroscopy (EDS). SEM micrographs were obtained after sputtering samples with a 10–15 nm thick gold film.

Filtration experiments were carried out in a pilot scale filtration unit, which consists of a feed tank, a recirculation pump, a vacuum pump, and a membrane module, as schematically shown in Fig. 2. The recirculation pump ensures a continuous cross flow outside the membrane, while a vacuum pump applies the transmembrane pressure to drive the filtration and collect the permeate from the internal membrane channels. The membranes were placed in a 5 L module with the top side open. First, the permeability of the membrane was measured using pure deionized water to evaluate its performance at different transmembrane pressures. The permeate flux was measured gravimetrically. Then, 50 L of feeds with different solutes were filtered to evaluate membrane performances in terms of rejection. These experiments were run at a constant transmembrane pressure of 1 bar, and cross flow of 240 L h^{-1} for 15 min. Samples from the feed and permeate were taken at the beginning and during the experiments. Considering that it was expected to obtain an ultrafiltration membrane, it was selected for the retention study: three proteins (hemoglobin, bovine serum albumin, and whey protein) with different molecular weights; indigo blue, a dye present in many industrial wastewaters; and humic acid, a model compound for natural

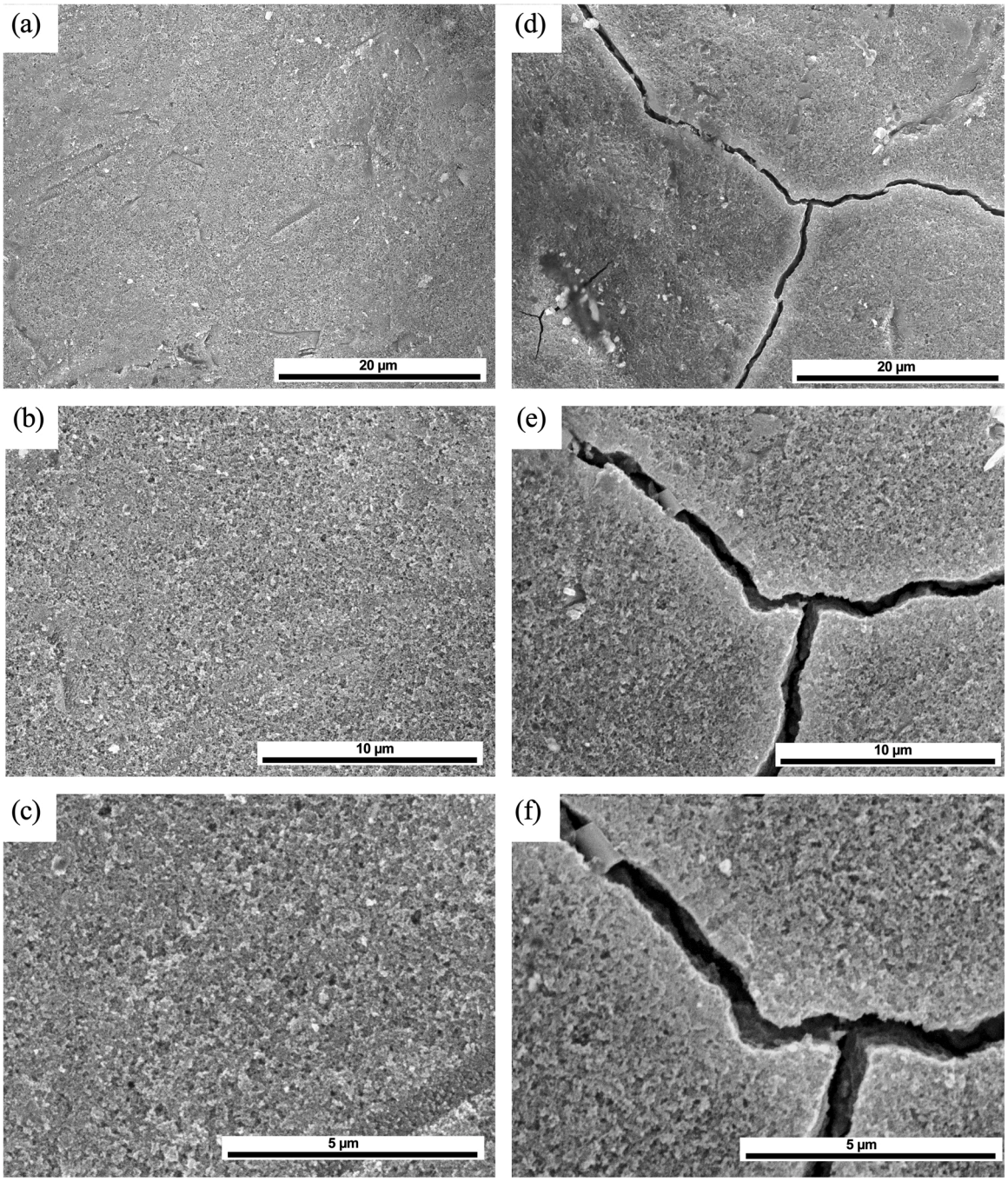

Fig. 6. Surface of the photocatalytic top layer sintered at the temperatures of (a,b,c) T and (d,e,f) T + 50 °C, at the magnifications of (a,d) 1.5k, (b,e) 5.5k, and (c,f) 10k. TiO_2 P25 dosage= 2%wt.

organic matter in the water and a model foulant.

For the experiments of polyethylene glycol (CAS 25322–68–3, Sigma-Aldrich) retention, solutions containing 1 g L^{-1} of PEG with molecular weights of 3, 8, 20, 35, 100, and 200 kg mol^{-1} were filtered. For humic acid (CAS 1415–93–6, Sigma-Aldrich) and indigo blue (CAS 482–89–3, Sigma-Aldrich) the initial feed concentration was 20 mg L^{-1}, while for bovine serum albumin (CAS 9048–46–8, >98%, Sigma-Aldrich), hemoglobin from bovine blood (CAS 9008–02–0, Sigma-Aldrich) and whey protein from cow milk (≥11% protein basis, Sigma-Aldrich), 1 g L^{-1} was used. In all the tests, the initial pH was adjusted to 7, with solutions of HCl and NaOH.

The PEG and proteins concentration in retentates and permeates were determined by size exclusion chromatography (SEC) using an isocratic Agilent 1100 pump (Agilent, CA, USA) equipped with an evaporative light scattering detector ELSD D 2000 (Mandel Scientific, Canada). A gel permeation chromatography (GPC) column (300 ×7.8 mm) PolySep-GFC-P 4000 (Phenomenex, CA, USA) was used with water as the mobile phase, flow rate of 1 mL min^{-1}, and injection volumes of 20 µL. The concentrations of humic acid and indigo blue were determined considering the absorbance of the samples at 254 and 660 nm, respectively, measured with the UV–vis spectrophotometer Cary 50 (Agilent, CA, USA).

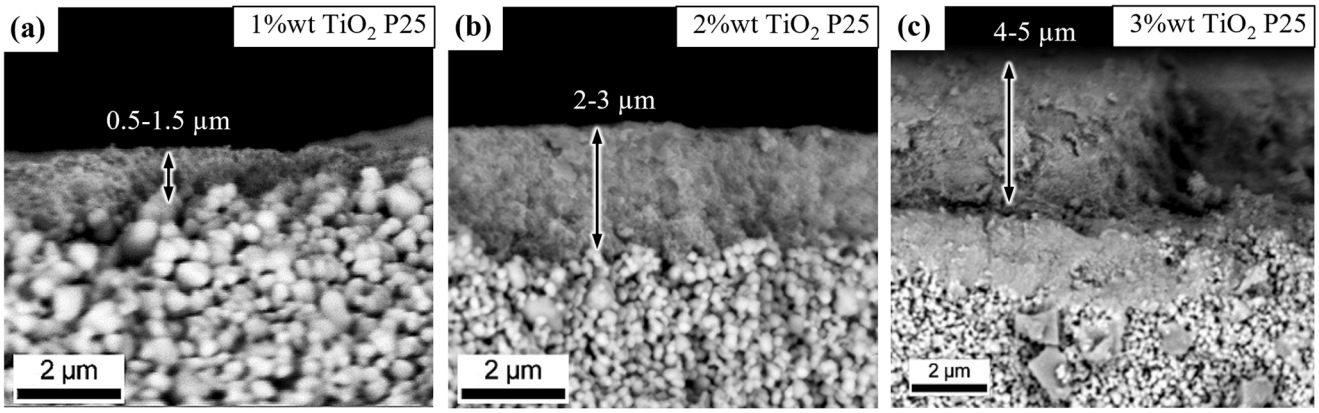

Fig. 7. Cross section of the membranes obtained with different TiO_2 P25 dosages and fired at temperature T.

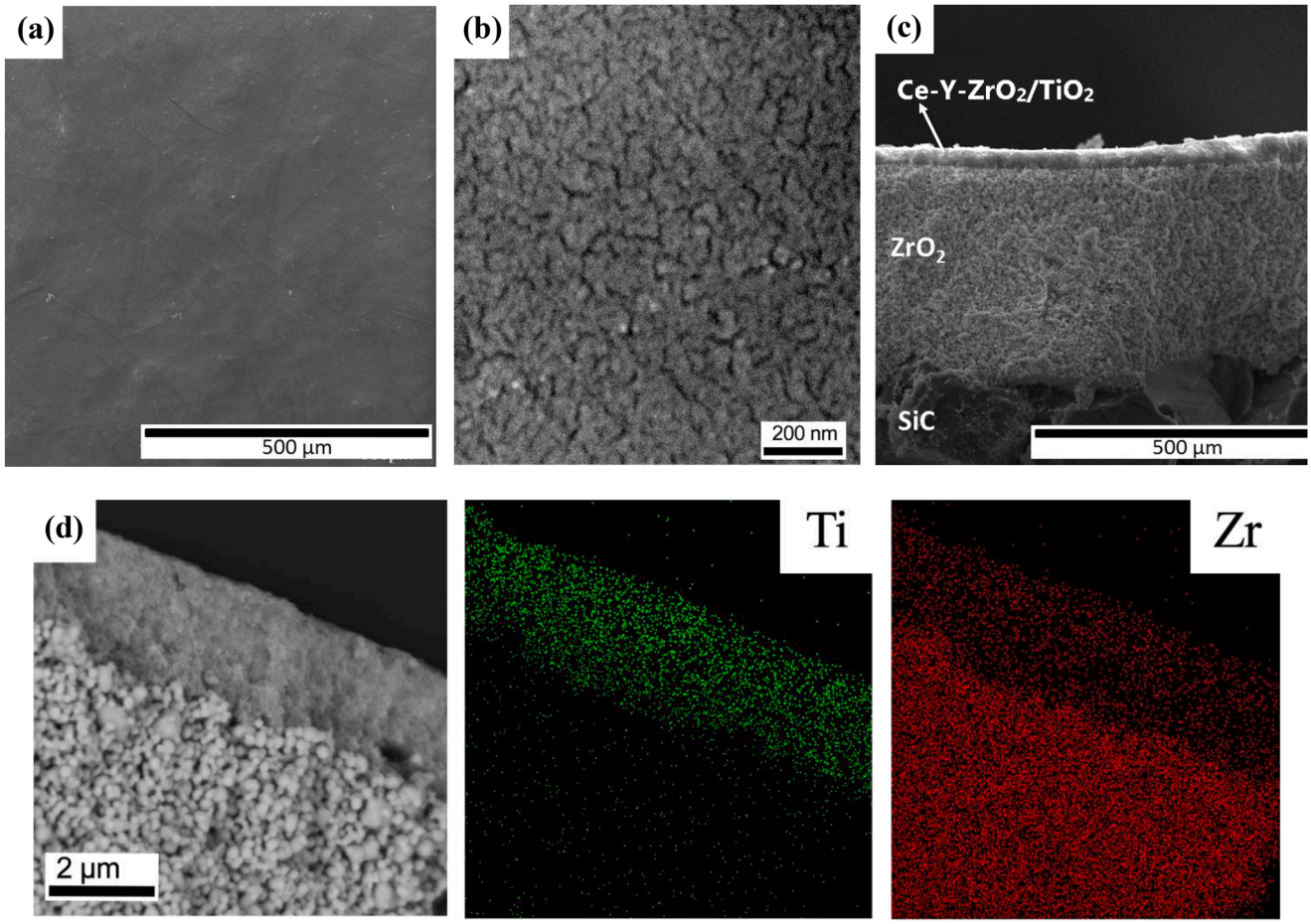

Fig. 8. SEM images of the photocatalytic membrane (a) surface, (b) surface at higher magnification, and (c) cross-section showing the SiC support, the ZrO_2 intermediate layer, and the Ce-Y-ZrO_2/TiO_2 top layer. (d) EDS elemental mapping of the cross section of the membrane.

2.3. Photocatalytic tests

2.3.1. Batch experiments and filtration with recirculation

The photocatalytic activity of the developed membrane was firstly evaluated in batch tests. For that, a membrane piece (4 cm length by 4 cm width) was placed into a 250 mL beaker containing 50 mL of an aqueous solution with 10 mg L^{-1} of phenol or humic acid. This system was then placed in a sunlight simulator SunTest XLS+ (Atlas-Ametek, IL, USA), located in Plataforma Solar de Almería-CIEMAT (Almería, Spain), and irradiated by a xenon lamp, with a daylight filter, that provided a total light radiation of 365 W m^{-2} (300–800 nm), of which 30 W m^{-2} was UV radiation (300–400 nm), under continuous ventilation to keep the temperature at 25 °C. Samples were collected in specific intervals. HA and phenol quantification were determined, respectively, by UV-spectroscopy, as described above, and by ultra-performance liquid chromatography (UPLC). For that, a UPLC 1200 device (Agilent, CA, USA), with a UV-DAD detector and a Poroshell 120 EC-C18 column (3.0 × 50 mm) was used. The eluent was 95% water with 25 mM of formic acid and 5% acetonitrile at 1 mL min^{-1}. The injection volume was 100 µL at a temperature of 30 °C. Samples were filtered through a

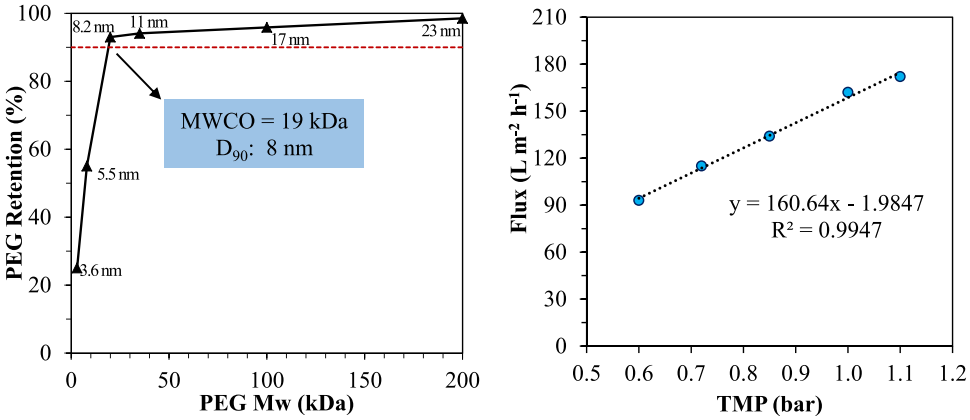

Fig. 9. (a) PEG retention of the photocatalytic membrane and their correspondent pore diameter calculated by Eq. 1. (b) Pure water flux of the membrane at different transmembrane pressures (TMP).

Table 2
Retention of selected compounds for the filtration at 1 bar with the photocatalytic membrane. Initial feed concentrations: 20 mg L^{-1} for humic acid, indigo blue, and 1 g L^{-1} for bovine serum albumin, hemoglobin, and whey protein.

Compound	MW (kDa)	Isoelectric point [36,84,86,87]	Charge at pH 7	Retention (%)
Humic Acid	4.7 – 30.4	3	negative	100
Indigo blue	0.262	N.A.	neutral	100
Bovine Serum Albumin	66	4.7	negative	92
Hemoglobin	64.5	5–7	negative	87
Whey protein (milk)	14–150	4.5	negative	87

hydrophobic PTFE 0.2 μm (Millipore, MA, USA) syringe filter prior to analysis. In order compare the activity of the photocatalytic membrane with the photo-Fenton reaction and the possibility to combine both processes, a series of experiments was carried out under the same conditions described above, except in the tests with phenol combined to: (i) Fe^{2+}, as a negative control experiment; (ii) Fe^{2+} and H_2O_2, a homogeneous photo-Fenton reaction; (iii) Fe^{2+} and the photocatalytic membrane. In these experiments, the H_2O_2 concentration was 50 mg L^{-1}, while the Fe^{2+} concentration was 5.5 mg L^{-1}, added as iron(II) sulfate heptahydrate ($FeSO_4.7\ H_2O$, CAS 7782–63–0, Sigma-Aldrich, >98%).

In the photocatalytic experiments with recirculation of the permeate, the filtration set-up showed in Fig. 2 was used, with the membrane module placed inside the solar simulator chamber described above. The initial feed volume was 5 L and the concentrations of phenol and humic acid were 10 mg L^{-1} in both cases. Samples of the retentate and permeate phases were collected and analysed by the same above-described procedures.

2.3.2. *Anti-fouling assessment by humic acid filtration*

The fouling behaviour of the photocatalytic membrane was investigated by filtering solutions of humic acid (20 mg L^{-1}, pH 5) in concentration experiments (no recirculation of the permeate) with the set-up, schemed in Fig. 2, placed inside a solar simulator described in the sub-Section 2.3.1. For that, the permeate flow and the HA concentration were measured during filtration. Four types of experiments were performed to investigate the membrane fouling. First, it was carried out separately the filtrations in the dark and under light irradiation. Then, a test with 1 h intervals of filtration in the dark combined with 1 h of light irradiation was carried out. In the last experiment, the filtration was performed initially under dark, until the membrane was fouled; then, the filtration was continued under light irradiation. After each experiment, the membrane was cleaned with a NaOH solution (pH 10), then with an HCl solution (pH 3), and finally rinsed exhaustively with distilled water. This procedure was performed only to guarantee the same initial conditions, the developed membranes should be self-cleaning under light irradiation, which means that in an actual operation, the chemical cleaning is avoided or performed less frequently compared to non-catalytic membranes.

3. Results and discussion

3.1. *Characterization of the Zr/Ti sols*

A homogeneous and defect-less top layer is the basic premise for achieving a selective and high-quality ceramic membrane. To this aim, the coating sols were optimized to avoid the zirconia phase transformation from monoclinic to tetragonal, since the volume variation in this transformation can easily generate cracks during membrane sintering [57]. Yttrium and titanium were therefore added to the zirconia sols as doping elements to stabilize the ZrO_2 tetragonal phase. These sols were dried, and the resulting gels were calcined at the temperature T, being T in the range 400–700 °C. Analysing the X-ray diffractograms of the unsupported membrane (Fig. S.2), the pure Ce-ZrO_2 sample presented 90%wt of the monoclinic and 10%wt of the tetragonal phases. By adding 20%mol of Ti into the Zr sols, Ce-ZrO_2/TiO_2 (Zr:Ti=8:2), the tetragonal phase increased to 30%wt and TiO_2 patterns was not observed in the XRD diffractogram, as reported elsewhere [50]. It is known that the addition of Ti, up to 40%mol, to Zr sols results in the formation of a solid solution of Ti into zirconia crystals, favouring the tetragonal polymorph [47]. In order to fully stabilize the tetragonal zirconia phase, yttrium was added to the Zr/Ti gels (Fig. S.2) achieving a final concentration of 8%mol Y_2O_3, as described in the literature for producing tetragonal yttria-stabilized zirconia (YSZ) [57], which can be heated up to 1000 °C without any phase transformation [58].

Therefore, to fabricate the photocatalytic membrane, the sol with a Zr:Ti molar ratio of 8:2 and with 8%molar of Y_2O_3 was chosen. The particle size analysis of this sol (Fig. 3) indicated nanosized particles between 2 and 10 nm, adequate for producing small pores ultrafiltration membranes. However, since the ZrO_2 intermediate layer on the SiC support has a pore size of 60 nm, it was required to add 2%wt of TiO_2 P25 nanoparticles to the coating fluid in order to avoid its excessive infiltration into the support void spaces. Moreover, the addition of solid particles into the gel network allows increasing strength and ductility of the supported layer, avoiding the gel to crack during the drying and early stage of sintering [55]. As shown in Fig. 3, the addition of TiO_2 P25 particles led to the formation of agglomerates of 100–1000 nm of diameter, as expected for dispersions in water [59].

In order to investigate the effect of sintering temperature on the phase composition, the optimised mixture of Ce-Y-ZrO_2/TiO_2 sol and the

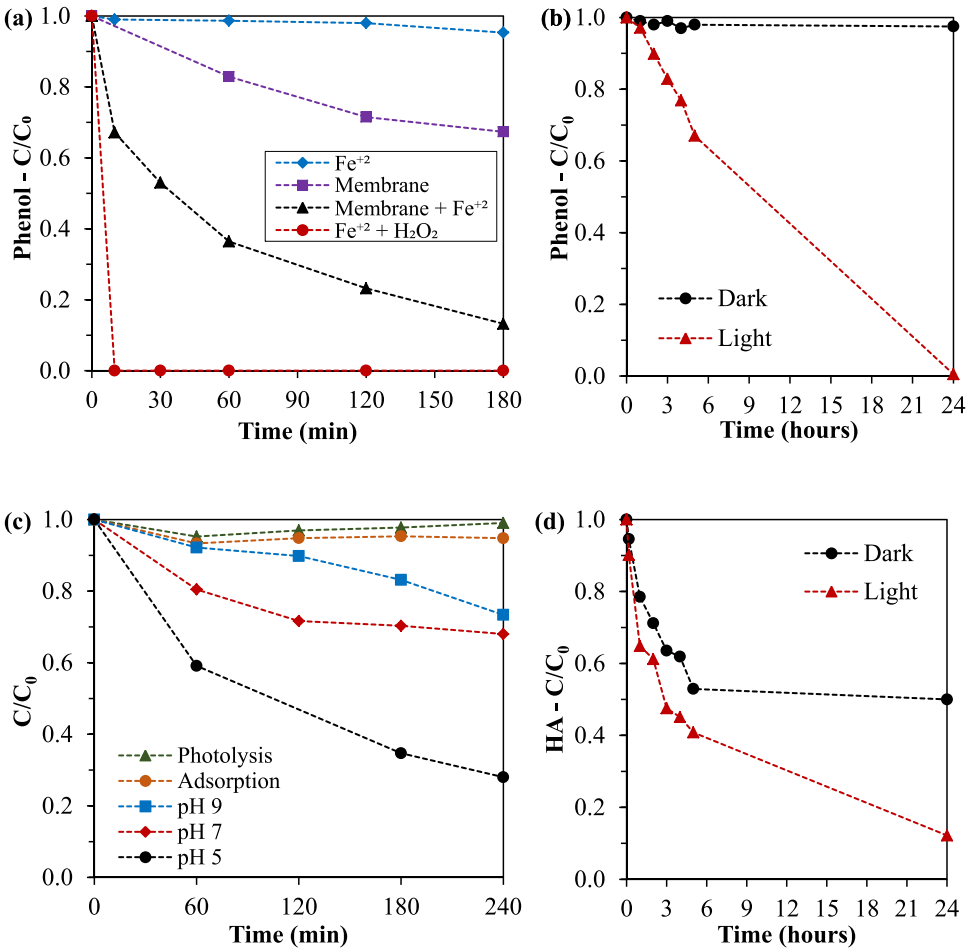

Fig. 10. Degradation of phenol in (a) batch experiments and in (b) filtration with recirculation. Initial phenol concentration $C_0 = 10$ mg L^{-1}, pH 3. Degradation of humic acid in (c) batch experiments and in (d) filtration with recirculation. Initial HA concentration 20 mg L^{-1}, pH 5.

dried coating fluid were calcined in three different temperatures in the range from 400° to 700°C, reported as T-50, T, and T + 50 °C due to confidentiality issues. The XRD analysis of the obtained unsupported membranes (Fig. 4) indicated that the complex system affects the normal behaviours of the single components as described in the following. a) It is known that the presence of Ti causes the increase of zirconia crystallization temperature from 400° to 550°C [47,50], which allows sintering the material at higher temperatures without losing the small pores. In fact, a firing temperature of T-50 °C was not high enough to promote the crystallization of zirconia. b) TiO_2 was present with both polymorphs, anatase and rutile, for all the tested firing temperatures, nevertheless, as it can be seen in Table 1, the ratio between anatase and rutile phases for all firing temperatures was 7:1, higher than the raw AEROXIDE® TiO_2 P25 ratio of 4:1 [60,61], suggesting the firing process of the complex system favoured the phase modification from anatase to rutile (thermodynamically stable polymorph) but avoiding the complete transformation expected for T > 600 °C [62], probably for a sort of stabilization effect carried out by Zr presence [47,63]. At the end of these experiments, the temperature of T-50 °C was discarded since it was not enough to promote the crystallization of the zirconia phase, required for the photocatalytic activity. **In** Table 1, it can also be observed that in the unsupported membrane (Ce-Y-ZrO_2/TiO_2 +TiO_2 P25) the Zr:Ti molar ratio, which was 8:2 (8.6:1.4 in weight) in the Zr/Ti gel, went to 1.2:8.8 (1.8:8.2 in weight).

The optical characterization of the fired Ce-Y-ZrO_2/TiO_2 gels (Fig. 5a) was used to estimate the band gaps of these samples though a Tauc's plot. Two band gaps were observed, one around 2.5 and the other around 3.6 eV. The first one can be explained by the cerium presence, as Ce promotes a red shift of the absorption within the visible region, as reported for Ce-doped zirconia [53] and titania [64]. The addition of a small amount of cerium introduces intra band gap states that act as a bridge between the valence and the conduction band of zirconia, allowing the absorption of low-energy photons in a double jump mechanism [53]. This shift reaches the visible-light region allowing this photocatalyst to work efficiently under solar light or visible LEDs irradiation [65,66]. The band gap around 3.6 eV is explained by the fact that the addition of Ti to the ZrO_2 gel reduces the pristine zirconia band gap (c.a. 5.0 eV [51]) due to the inclusion of Ti ions into the ZrO_2 lattice [67].

Regarding the unsupported membranes (Ce-Y-ZrO_2/TiO_2 gel with TiO_2 P25 nanoparticles), their optical behaviour is shown on Fig. 5b. Again, two values of band gap were observed, one around 2.4–2.5 eV caused by the Ce-doping, and another one around 3.0–3.1 eV, which correspond to the values of titania anatase (3.2 eV) and rutile (3.0 eV) [68]. The band gap of zirconia was not observed, probably because TiO_2 P25 particles hide the ZrO_2 signal, the unsupported membranes contain around 80%wt of TiO_2.

From the zeta potential measurements of the unsupported membranes (Fig. 5c), it can be observed that the isoelectric point of these powders is between 3.5 and 5.5, corresponding to the values expected for Ce-ZrO_2, 3.5 [52], and TiO_2, 3.5–6.5 [69]. The isoelectric point moves towards higher pH values when increased the firing temperature from T to T + 50 °C. It is known that for TiO_2 nanoparticles synthetized by a sol-gel route [70], residual carbon species from the synthesis forms carbonate groups at the surface of the mixed oxide that shift its isoelectric point to lower pH values [71]. Therefore, higher sintering

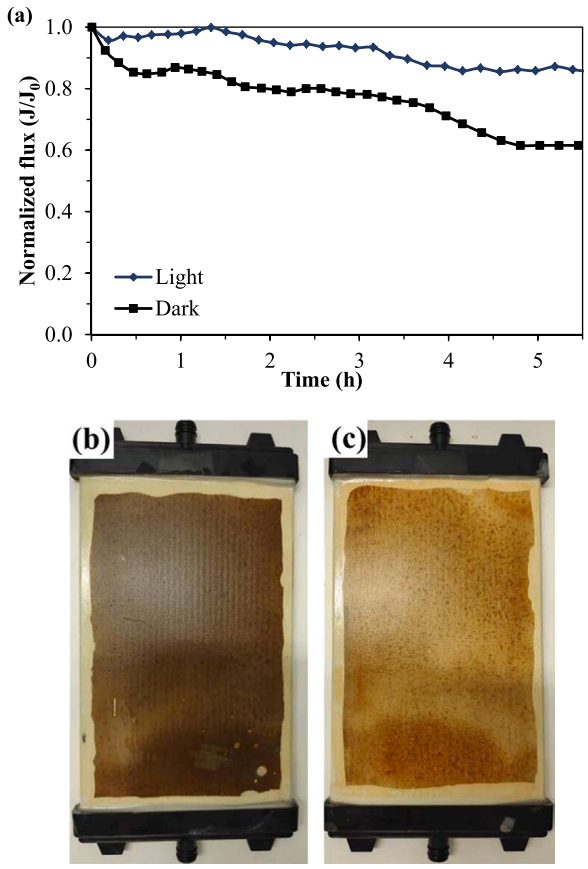

Fig. 11. (a) Normalized flux during humic acid filtration in the dark, under light irradiation. Pictures of the membrane after HA filtration (b) in the dark and (c) under irradiation.

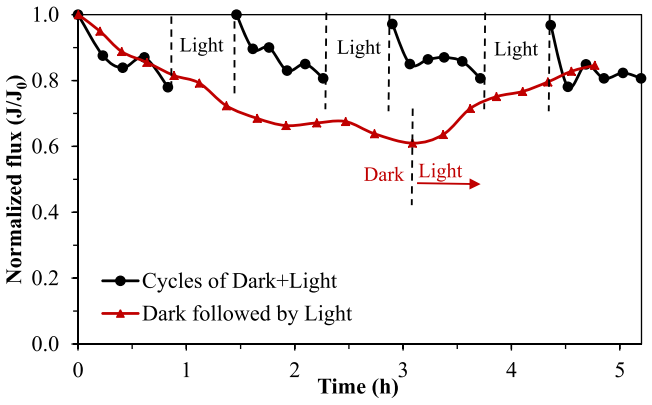

Fig. 12. Normalized permeate flux (J/J_0) for the HA filtration experiments with dark and light intervals.

temperatures removes these carbonate groups and increase the isoelectric point. This effect could be considered during the process of membrane fabrication because the choice of the firing temperature could allow tailoring the membrane surface charge in two directions: improving the retention of oppositely charged molecules or improving the membrane antifouling properties maintaining the membrane at the same charge of fouling compounds (humic substances are typically negatively charged) [72]. For our purposes, a firing temperature of T is preferred to fabricate a membrane with a strong negative charge in a wider range of pH, but it should be also considered the possible effect of the temperature on the layer formation. Therefore, the two temperatures of T and T + 50 °C will still be investigated in the following.

3.2. Optimization of the coating

Once the unsupported membranes were characterized, the coating and layer formation processes to fabricate the photocatalytic membrane were investigated. For that, two sintering temperatures were tested, T and T + 50 °C. From the SEM images of the obtained membranes (Fig. 6), it can be seen that at T + 50 °C the top layer presented a considerable amount of cracks, which even led to the peeling of the top layer. As shown in Table 1, no phase transformations were observed after sintering at the temperatures of T and T + 50 °C, but there was an increase in the tetragonal ZrO_2 and anatase TiO2crystallite sizes, therefore, the cracks observed at 600 °C were most likely caused by the dimensional change of the particles in the densification process occurring during the heating. The volumetric shrinking of the top layer generates tensile stresses that cause the layer to crack [73]. On the other side, at the sintering temperature of T, the membrane obtained was crack-free and no peeling was observed, this temperature was thus chosen for sintering the membrane after deposition of the top layer.

Fig. 7 reports the top layer morphology and thickness obtained with the dosages of 1%, 2%, 3%, 5%, and 10%wt of TiO_2 P25 nanoparticles added to the coating fluid. The dosage of 1%wt led to a thin layer not completely homogeneous and this could compromise the separation capability of the membrane. On the other hand, with 5%wt of TiO_2, the layer was too thick and with cracks, as expected because of the tensile stresses cause deformation of the layer in the plane and the consequent spontaneous formation of cracks [74–76]. In addition, the suspension prepared with 10%wt TiO_2 nanoparticles was not stable. In conclusion, the dosages of 1%, 5%, and 10%wt were discarded for the fabrication of the membrane.

The best membrane, homogeneous and defect-free, was obtained with 2%wt of TiO_2 P25 in the coating fluid, therefore this dosage was chosen for fabricating the top layer.

3.3. Characterization of the membrane

Fig. 8a shows the membrane top layer, as prepared with the optimised parameters. The surface is smooth and without defects, such as cracks and pinholes. At the higher magnification (Fig. 8b), it is possible to observe the good sintering of the nanoparticles. In Fig. 8c, the typical multilayer section of the asymmetric membrane can be observed: the macroporous SiC support, the mesoporous ZrO_2 intermediate layer, and the Ce-Y-ZrO_2/TiO_2 photocatalytic top layer, which looks uniform and appropriately joined with the underneath ZrO_2 layer. The penetration of the coating fluid into the intermediate layer pores was not significant, as verified by the EDS elemental mapping of the membrane cross-section (Fig. 8d), where it is possible to verify the top layer composition and the homogeneity of the membrane layer, showing a thickness of ~2 μm.

The molecular weight cut-off (MWCO) of the developed membrane was estimated using the polyethylene glycol (PEG) retention curve (Fig. 9a), a common procedure for ultrafiltration membranes [77,78]. Therefore, a MWCO of 19 kDa was obtained, which corresponds to the PEG molecular weight (MW) for which 90% of the molecules are retained during filtration. The pore size of the membrane can be estimated using a correlation to convert the PEG molecular weight into pore diameter (Eq. 1)[14,38].

$$d_p = 0.085 \cdot (MW)^{0.46} \quad (1)$$

From this equation, it is possible to conclude that 90% of the pores (D_{90}) of the developed membrane are below 8 nm of diameter and 50% of the pores (D_{50}) are below 5 nm. The estimated average pore size is 6 nm. Based on these PEG retention data, this system can be classified as an ultrafiltration membrane [1], having pore sizes in the mesoporous range [55].

Table 3
Comparison of photocatalytic ceramic membranes.

Reference	Top layer	Support (Pore size)	Pore size (nm)	Clean water permeability ($Lm^{-2}h^{-1}bar^{-1}$)	Photocatalytic test	
					Contaminant	Light source
This work	Ce-Y-ZrO_2/ TiO_2	SiC (15 μm) + ZrO2 (60 nm)	6	160	Phenol and Humic acid	Simulated sunlight (300–800 nm)
Taavoni-Gilan et al. [35]	TiO_2/ZrO_2	α-Al_2O_3 + TiO_2	4	5	Methyl violet dye	UV
Goei et al. [26]	TiO_2	Al_2O_3	< 10	155	Rhodamine B	UV (365 nm)
Goei et al. [27]	Ag-TiO_2	Al_2O_3	N.A.	123	Rhodamine B + Bacteria	
Mendret et al. [28]	TiO_2/ Al_2O_3	Al_2O_3 (200 nm)	< 200	200	Acid Orange 7	
Alias et al. [18]	TiO_2	Al_2O_3 /SiO_2	N.A.	50–100	Humic acid	UV
Zhang et al. [29]	TiO_2	Al_2O_3 (200 nm)	50–100	400	Direct Black 168	UV(365 nm)
Zhang et al. [37]	Si- TiO_2		< 60	N.A.		
Manjumol et al. [36]	TiO_2	Al_2O_3 (1 μm)	11	215	Methylene blue	UV

The retentions of selected compounds are shown in Table 2, in which it is possible to observe the high retentions of humic acid, proteins, and indigo blue. Since the developed membrane has a MWCO of 19 kDa, the sieving mechanism, in which compounds with MW higher than membrane pore size are retained on the membrane surface [79], can explain the good retentions of bovine serum albumin, hemoglobin, and whey protein. However, the sieving mechanism does not seem to be the only one driving the filtration process, as small molecules as indigo blue or the low MW fraction of the humic acid, whose dimensions should be below the membrane MWCO, are totally retained by the membrane [23]. Actually, also interfacial interactions need to be taken into account, namely electrostatic repulsions (charge effect) and hydrophobic–adsorptive interactions [80] established between membrane surface and the solutes to be separated [79]. Indigo blue is a hydrophobic compound insoluble in water [81]: its retention is caused by its strong adsorption onto oxide surfaces [82] and by the consequent formation of a cake blocking the membrane pores [83]. However, the retention of HA can be explained by sieving effect and by the electrostatic repulsion generated by the negatively charged humic acid [84,85] and the negatively charged membrane surface at the filtration pH (Fig. 5**c**).

The flux of pure (non-fouling) water was measured at different transmembrane pressures (Fig. 9b), resulting in a permeability of 160 L m^{-2} h^{-1} bar^{-1}, similar to the ones reported in the literature for zirconia/titania non-catalytic membranes: Larbot et al. [88] fabricated ZrO_2 membranes with pore sizes from 6 to 10 nm on α-Al_2O_3 supports, achieving water permeabilities from 175 to 210 L m^{-2} h^{-1} bar^{-1}, while Li et al. [55] obtained permeabilities of 128–180 L m^{-2} h^{-1} bar^{-1} with their TiO_2 membranes of pore sizes from 3 to 5 nm on a ZrO_2 support.

3.4. Photocatalytic activity

The photocatalytic activity of the unsupported membrane (Ce-Y-ZrO_2/TiO_2 + TiO_2 P25) was evaluated with the photodegradation of phenol (10 mg L^{-1}) in a solar simulator (Fig. S.3**a**), following a standard procedure [30,89,90] taking advantage from the fact that phenol does not present significant adsorption nor direct photolysis. The experiment carried out with pure TiO_2 P25 results in 100% of phenol degradation in 150 min, but the unsupported membrane promotes 70% of degradation at the same time, confirming the photoactivity of the system. Compared to these data, the catalytic activity of the membrane measured in batch experiments at pH 3 and 6 (reported in Fig. S.3**b**) is much more limited, nevertheless the results are promising when considering that the membrane fabrication led to the reduction of the surface area available for the catalytic process. Moreover, the photocatalytic membrane has several advantages compared to the powdery catalysts, mainly the elimination of a separation process to recover the photocatalytic nanoparticles dispersed in water [66,91].

The mechanism governing the photodegradation of organic compounds with TiO_2 has been extensively described in the literature [92,93], whereas only few works deal with the explanation of Ce-ZrO_2 activity [51,53,94], but in all cases, the semiconductor oxides (Ce-ZrO_2 or TiO_2) absorb photons promoting the photo-induced h^+/e^- charge separation. Once formed, valence band holes (h^+) can undergo three reactions: i) directly oxidize organic molecules (Eq. (2)); ii) oxidize H_2O molecules generating $^{\bullet}OH$ radicals (Eq. (3)); iii) oxidize -OH groups adsorbed in TiO_2 surface to produce $^{\bullet}OH$ radicals (Eq. (4)). Once formed, the hydroxyl radicals successively oxidize the organic molecules at the catalyst surface. The superoxide anion radicals ($^{\bullet}O_2^-$), generated by photo-induced electrons (e^-) in the valence band, could also participate in degrading the organic compounds [52].

$$h^+ + \quad \text{organic molecule} \rightarrow \quad \text{oxidized product} \tag{2}$$

$$H_2O + h_{VB}^+ \rightarrow {}^{\bullet}OH + H^+ \tag{3}$$

$$-Ti - OH + h_{VB}^+ \rightarrow -Ti^+ + {}^{\bullet}OH \tag{4}$$

A possibility to accelerate the contaminants abatement by increasing the production of reactive $^{\bullet}OH$ species is to irradiate the TiO_2 present in the membrane [95], which promotes the in-situ generation of hydrogen peroxide that, in the presence of Fe^{+2} ions, catalyses phenol degradation reaction, in a photo-Fenton process (Eqs. (5–7)).

$$Fe^{2+} + H_2O_2 \rightarrow Fe^{3+} + OH^- + {}^{\bullet}OH \tag{5}$$

$$Fe^{3+} + H_2O_2 \rightarrow Fe^{2+} + H^+ + {}^{\bullet}O_2H \tag{6}$$

$$Fe^{3+} + H_2O \xrightarrow{h\nu} Fe^{2+} + H^+ + {}^{\bullet}OH \tag{7}$$

As it can be seen in Fig. 10**a**, a great increase of phenol degradation was observed adding Fe^{+2} ions to the phenol solution. In this condition, the generated H_2O_2 catalyses the phenol degradation by reacting with Fe^{2+} ions to generate $^{\bullet}OH$ radicals [96], while Fe^{3+} ions are reduced to Fe^{2+} completing the Fenton cycle [97]. As a positive control experiment, a homogenous photo-Fenton experiment (Fe^{2+}+H_2O_2) without the membrane, resulted in a fast phenol degradation, as expected [32]. On the other hand, in a negative control experiment, no phenol degradation was observed in the test with only Fe^{2+} added to the system, since no H_2O_2 nor photocatalyst was present.

In Fig. 10**b**, it is shown the concentration of phenol in the feed during filtration experiments with recirculation of the permeate. Since phenol is not retained by the developed membrane because of its very small size, its concentration in the permeate remained constant in the dark filtration, but when the irradiation started its concentration decreased thanks to the photocatalytic action of the membrane.

Regarding the degradation of humic acid (HA), in batch experiments (Fig. 10**c**), there was no significant adsorption or photolysis, but a clear effect of the photodegradation carried out by the membrane was observed. Lower pH values favoured the HA degradation because in acid

media, ZrO_2/TiO_2 and HA become less negative, reducing the electrical repulsion between them and, therefore, increasing the HA adsorption into the catalyst surface, as reported in the literature [52,98].

In filtration experiments with recirculation of the permeate (Fig. 10**d**), HA is retained in large amount by the membrane thanks to the cooperative effect of membrane retention and cake formation, as demonstrated by the HA concentration decrease with time in the dark experiment. In the filtration under light irradiation, a higher removal of HA was observed, confirming the photocatalytic activity of the membrane. In summary, these results demonstrate the potential antifouling effect of the developed membrane, which is able in degrading efficiently organic compounds (and retentates) under solar light irradiation taking advantage of photo-Fenton process.

3.5. Anti-fouling properties

Humic acid (HA) was chosen as a model compound for simulating the presence of natural organic matter that is a major foulant during ultrafiltration of surface and wastewater [17,18]. The normalized permeate flux (J/J_0) measured in HA filtration using the photocatalytic membrane in the dark and under visible light irradiation is shown in Fig. 11**a**. It can be seen that the initial flux recorded in the dark has a fast decline that continue to reduce slower as the filtration continues. This trend can be explained considering the fouling caused by the HA adsorption on the membrane and blockage of the pores, with the formation of a cake- or gel-like layer on the membrane surface, as reported by other authors [18,99]. This layer could not be removed by water rinsing and required a chemical cleaning with a NaOH solution. On the other hand, the experiments carried out under simulated sun light exhibited a lower flux decline. After 5 h of filtration, the flux reduced to 85% of the initial value (119 L m^{-2} h^{-1}), while for the filtration in the dark the flux was reduced to 60% of the initial one (105 L m^{-2} h^{-1}) in the same time interval. This result can be explained considering two phenomena, both affecting the tendency of the membrane to foul [28]: the defouling caused by the photocatalytic degradation of HA on the membrane surface, expected considering the results of the previous experiments, and causing the decrease of HA in the retentate phase reported in Fig. S.4, and the photo-induced super-hydrophilicity (PSH) of TiO_2 [26,27]. In fact, the membrane under light irradiation presents a higher hydrophilicity that favours higher fluxes and prevents fouling tendency compared to the membrane in the dark. The fouling effect can be visually observed by comparing the membrane after the HA filtration in the dark (Fig. 11**b**) and under irradiation (Fig. 11**c**).

In order to confirm and proof the self-cleaning properties of the membrane, two operational conditions were tested (Fig. 12): a) approximately one-hour filtration in the dark alternated with 30 min irradiation upon simulated sun light in three following cycles, and b) the filtration carried out in the dark for the first 3 h and then under irradiation for the following 2 h. In the first experiment (case a), a strong flux decline was observed during the filtration in the dark caused by the HA fouling. As the membrane was irradiated, the original flux was recovered due to the HA degradation and cleaning of the membrane. In the second and third cycles of dark filtration and photo-induced cleaning, a slight decrease of the flux recovery was observed, but always 97% of the initial flux was reached after irradiation. In the second experiment (case b), the decrease of the normalised flux witnessed the membrane fouling observed during the 3 h of dark filtration, whereas the irradiation caused the flux recovery for the higher photo-induced surface hydrophilicity and cleaning of the membrane caused by the HA photodegradation.

For comparison, the performances of some ZrO_2 and TiO_2 UF photocatalytic membranes reported in literature are listed in Table 3. Apart some cases, the Ce-Y-ZrO_2/TiO_2 membrane developed in this work presents advantages with respect to most part of the membranes described in the list. In fact, in several works the photoactivity of the membranes was evaluated using dyes, although it is known that they can undergo to direct photolysis under UV-light irradiation creating misunderstanding and wrong evaluations on the real activity of the membranes [56]. Also, in several cases the use of pristine TiO_2 implies the use of UV-light to activate the photocatalyst. Finally, most part of the membranes present in the list exhibits a lower permeability with respect to the Ce-Y-ZrO_2/TiO_2 membrane developed in this work, although other membranes showed similar pore size range. It seems that most part of the described advantages derives from the use of SiC as membrane support as it can enhance the capacity of the active layer. Moreover, the use of a Ce-doped catalyst allows the use of visible light that favours the use of solar light for membrane anti-fouling and self-cleaning applications.

4. Conclusions

In the present work, a photocatalytic Ce-Y-ZrO_2/TiO_2 ultrafiltration membrane on ZrO_2/SiC supports was successfully prepared by a modified sol-gel process. The top active layer was uniform and defect-free with a thickness of 2 μm. Its composition was tetragonal zirconia, anatase and rutile titania. The membrane presented a MWCO of 19 kDa, equivalent to an average pore size of 6 nm, and a high clean water permeability, 160 L m^{-2} h^{-1} bar^{-1}. High retention of proteins (bovine serum albumin, whey protein, and hemoglobin), indigo dye, and humic acid were achieved, favoured by the high hydrophilicity and negative surface charge of the membrane. In photocatalytic experiments, the developed membrane was able to degrade phenol and humic acid under simulated sunlight irradiation. In humic acid filtration tests, the membrane presented better anti-fouling properties (smaller flux decline) and higher permeate flux under irradiation compared to the filtration in the dark, as a result of the HA photodegradation and the light-induced super-hydrophilicity of the TiO_2 top layer. Consequently, the membrane can operate longer without chemical cleaning, reducing the operational cost, and the process footprint. In addition, the membrane presented self-cleaning properties, being able to recover up to 97% of the original flux by exposing the membrane to simulated sun light. In conclusion, these results point out the relevance in deepening the investigations in developing applications of the photocatalytic membranes in innovative treatments for dinking and wastewaters by combining filtration and advanced oxidation processes for the abatement of contaminants of emerging concern in the presence of natural organic matter.

CRediT authorship contribution statement

Fabrício Bortot Coelho: Conceptualization, Methodology, Investigation, Writing – original draft, Writing – review & editing, Project administration. **Dennis Deemter:** Conceptualization, Methodology, Investigation, Writing – review & editing. **Victor M. Candelario:** Methodology, Writing – review & editing, Project administration, Supervision. **Vittorio Boffa:** Methodology, Investigation, Supervision. **Sixto Malato:** Conceptualization, Methodology, Writing – review & editing, Project administration, Supervision. **Giuliana Magnacca:** Conceptualization, Methodology, Writing – original draft, Writing – review & editing, Project administration, Supervision.

Declaration of Competing Interest

The authors declare that they have no known competing financial interests or personal relationships that could have appeared to influence the work reported in this paper.

Acknowledgments

This paper is part of a project that has received funding from the European Union's Horizon 2020 research and innovation programme under the Marie Skłodowska-Curie grant agreement No 765860.

Appendix A. Supporting information

Supplementary data associated with this article can be found in the online version at doi:10.1016/j.jece.2021.106671.

References

[1] Z. He, Z. Lyu, Q. Gu, L. Zhang, J. Wang, Ceramic-based membranes for water and wastewater treatment, Colloids Surf. A Physicochem. Eng. Asp. 578 (2019), 123513, https://doi.org/10.1016/j.colsurfa.2019.05.074.

[2] M.A. Shannon, P.W. Bohn, M. Elimelech, J.G. Georgiadis, B.J. Marin, A.M. Mayes, Science and technology for water purification in the coming decades 452 (2008) 301–310, https://doi.org/10.1038/nature06599.

[3] M. Campinas, R.M.C. Viegas, R. Coelho, H. Lucas, M.J. Rosa, Adsorption/coagulation/ceramic microfiltration for treating challenging waters for drinking water production, Membr 11 (2021), https://doi.org/10.3390/membranes11020091.

[4] S. Li, C. Wei, P. Wang, P. Gao, L. Zhou, G. Wen, Zirconia ultrafiltration membranes on silicon carbide substrate: microstructure and water flux, J. Eur. Ceram. Soc. 40 (2020) 4290–4298, https://doi.org/10.1016/j.jeurceramsoc.2020.04.020.

[5] Q. Jiang, J. Zhou, Y. Miao, S. Yang, M. Zhou, Z. Zhong, W. Xing, Lower-temperature preparation of SiC ceramic membrane using zeolite residue as sintering aid for oil-in-water separation, J. Memb. Sci. 610 (2020), 118238, https://doi.org/10.1016/j.memsci.2020.118238.

[6] H. Qin, W. Guo, X. Huang, P. Gao, H. Xiao, Preparation of yttria-stabilized ZrO_2 nanofiltration membrane by reverse micelles-mediated sol-gel process and its application in pesticide wastewater treatment, J. Eur. Ceram. Soc. 40 (2020) 145–154, https://doi.org/10.1016/j.jeurceramsoc.2019.09.023.

[7] Y. Feng, K. Wang, C. Davies, H. Wang, Carbon nanotube/alumina/polyethersulfone hybrid hollow fiber membranes with enhanced mechanical and anti-fouling properties, Nanomaterials 5 (2015) 1366–1378, https://doi.org/10.3390/nano5031366.

[8] A. Kayvani Fard, G. McKay, A. Buekenhoudt, H. Al Sulaiti, F. Motmans, M. Khraisheh, M. Atieh, Inorganic membranes: preparation and application for water treatment and desalination, Mater. (Basel) 11 (2018) 74, https://doi.org/10.3390/ma11010074.

[9] B. Hofs, J. Ogier, D. Vries, E.F. Beerendonk, E.R. Cornelissen, Comparison of ceramic and polymeric membrane permeability and fouling using surface water, Sep. Purif. Technol. 79 (2011) 365–374, https://doi.org/10.1016/j.seppur.2011.03.025.

[10] T. Tsuru, Inorganic porous membranes for liquid phase separation, Sep. Purif. Methods 30 (2001) 191–220, https://doi.org/10.1081/SPM-100108159.

[11] M.M. Pendergast, E.M.V. Hoek, A review of water treatment membrane nanotechnologies, Energy Environ. Sci. 4 (2011) 1946, https://doi.org/10.1039/c0ee00541j.

[12] X. Zhang, T. Zhang, J. Ng, D.D. Sun, High-performance multifunctional TiO_2 nanowire ultrafiltration membrane with a hierarchical layer structure for water treatment, Adv. Funct. Mater. 19 (2009) 3731–3736, https://doi.org/10.1002/adfm.200901435.

[13] C. Li, W. Sun, Z. Lu, X. Ao, S. Li, Ceramic nanocomposite membranes and membrane fouling: a review, Water Res 175 (2020), 115674, https://doi.org/10.1016/j.watres.2020.115674.

[14] D. da Silva Biron, V. dos Santos, M. Zeni, Ceram. Membr. Appl. Sep. Process. (2018), https://doi.org/10.1007/978-3-319-58604-5.

[15] G. Mustafa, K. Wyns, P. Vandezande, A. Buekenhoudt, V. Meynen, Novel grafting method efficiently decreases irreversible fouling of ceramic nanofiltration membranes, J. Memb. Sci. 470 (2014) 369–377, https://doi.org/10.1016/j.memsci.2014.07.050.

[16] A.W. Zularisam, A.F. Ismail, M. Sakinah, Application and challenges of membrane in surface water treatment, J. Appl. Sci. 10 (2010) 380–390, https://doi.org/10.3923/jas.2010.380.390.

[17] W. Yuan, A.L. Zydney, Humic acid fouling during ultrafiltration, Environ. Sci. Technol. 34 (2000) 5043–5050, https://doi.org/10.1021/es0012366.

[18] S.S. Alias, Z. Harun, I.S.A. Latif, Characterization and performance of porous photocatalytic ceramic membranes coated with TiO_2 via different dip-coating routes, J. Mater. Sci. 53 (2018) 11534–11552, https://doi.org/10.1007/s10853-018-2392-3.

[19] C. Zhang, J. Zhang, X. Min, M. Wang, B. Zhou, C. Shen, Kinetics of reductive acid leaching of cadmium-bearing zinc ferrite mixture using hydrazine sulfate, Jom 67 (2015) 2028–2037, https://doi.org/10.1007/s11837-015-1553-y.

[20] W.M. Clark, A. Bansal, M. Sontakke, Y.H. Ma, Protein adsorption and fouling in ceramic ultrafiltration membranes, J. Memb. Sci. 55 (1991) 21–38, https://doi.org/10.1016/S0376-7388(00)82325-X.

[21] B. Van der Bruggen, M. Mänttäri, M. Nyström, Drawbacks of applying nanofiltration and how to avoid them: A review, Sep. Purif. Technol. 63 (2008) 251–263, https://doi.org/10.1016/j.seppur.2008.05.010.

[22] X. Zhang, L. Fan, F.A. Roddick, Effect of feedwater pre-treatment using UV/H_2O_2 for mitigating the fouling of a ceramic MF membrane caused by soluble algal organic matter, J. Memb. Sci. 493 (2015) 683–689, https://doi.org/10.1016/j.memsci.2015.07.024.

[23] K. Staszak, Membrane processes, Phys. Sci. Rev. 2 (2017) 1–18, https://doi.org/10.1515/psr-2017-0142.

[24] N.F. Ishak, N.A. Hashim, M.H.D. Othman, P. Monash, F.M. Zuki, Recent progress in the hydrophilic modification of alumina membranes for protein separation and purification, Ceram. Int. 43 (2017) 915–925, https://doi.org/10.1016/j.ceramint.2016.10.044.

[25] G. Zhang, W. Jin, N. Xu, Design and fabrication of ceramic catalytic membrane reactors for green chemical engineering applications, Engineering 4 (2018) 848–860, https://doi.org/10.1016/j.eng.2017.05.001.

[26] R. Goei, T.-T. Lim, Asymmetric TiO_2 hybrid photocatalytic ceramic membrane with porosity gradient: effect of structure directing agent on the resulting membranes architecture and performances, Ceram. Int. 40 (2014) 6747–6757, https://doi.org/10.1016/j.ceramint.2013.11.137.

[27] R. Goei, T.T. Lim, Ag-decorated TiO_2 photocatalytic membrane with hierarchical architecture: photocatalytic and anti-bacterial activities, Water Res 59 (2014) 207–218, https://doi.org/10.1016/j.watres.2014.04.025.

[28] J. Mendret, M. Hatat-Fraile, M. Rivallin, S. Brosillon, Hydrophilic composite membranes for simultaneous separation and photocatalytic degradation of organic pollutants, Sep. Purif. Technol. 111 (2013) 9–19, https://doi.org/10.1016/j.seppur.2013.03.030.

[29] H. Zhang, X. Quan, S. Chen, H. Zhao, Y. Zhao, Fabrication of photocatalytic membrane and evaluation its efficiency in removal of organic pollutants from water, Sep. Purif. Technol. 50 (2006) 147–155, https://doi.org/10.1016/j.seppur.2005.11.018.

[30] S. Sanches, C. Nunes, P.C. Passarinho, F.C. Ferreira, V.J. Pereira, J.G. Crespo, Development of photocatalytic titanium dioxide membranes for degradation of recalcitrant compounds, J. Chem. Technol. Biotechnol. 92 (2017) 1727–1737, https://doi.org/10.1002/jctb.5172.

[31] S. Leong, A. Razmjou, K. Wang, K. Hapgood, X. Zhang, H. Wang, TiO_2 based photocatalytic membranes: a review, J. Memb. Sci. 472 (2014) 167–184, https://doi.org/10.1016/j.memsci.2014.08.016.

[32] J.P. Ribeiro, M.I. Nunes, Recent trends and developments in Fenton processes for industrial wastewater treatment – a critical review, Environ. Res. 197 (2021), https://doi.org/10.1016/j.envres.2021.110957.

[33] Y.G. Zhang, L.L. Ma, J.L. Li, Y. Yu, In situ fenton reagent generated from TiO_2/Cu_2O composite film: a new way to utilize TiO_2 under visible light irradiation, Environ. Sci. Technol. 41 (2007) 6264–6269, https://doi.org/10.1021/es070345i.

[34] C.P. Athanasekou, N.G. Moustakas, S. Morales-Torres, L.M. Pastrana-Martínez, J. L. Figueiredo, J.L. Faria, A.M.T. Silva, J.M. Dona-Rodriguez, G.E. Romanos, P. Falaras, Ceramic photocatalytic membranes for water filtration under UV and visible light, Appl. Catal. B Environ. 178 (2015) 12–19, https://doi.org/10.1016/j.apcatb.2014.11.021.

[35] A. Taavoni-Gilan, E. Taheri-Nassaj, M. Shamsipur, Synthesis of nanostructured titania/zirconia membrane and investigation of its physical separation and photocatalytic properties in treatment of textile industries wastewater, J. Iran. Chem. Soc. 15 (2018) 2759–2769, https://doi.org/10.1007/s13738-018-1463-3.

[36] K.A. Manjumol, S. Sankar, B.N. Nair, M. Midhun, P.A. Mohamed, K.G.K. Warrier, A novel approach to formulate high flux multifunctional ultrafiltration membranes from photocatalytic titania composite precursors on multi-channel tubular substrates, RSC Adv. 6 (2016) 58813–58822, https://doi.org/10.1039/c6ra14117j.

[37] H. Zhang, X. Quan, S. Chen, H. Zhao, Fabrication and characterization of silica/titania nanotubes composite membrane with photocatalytic capability, Environ. Sci. Technol. 40 (2006) 6104–6109, https://doi.org/10.1021/es060092d.

[38] V. Gitis, G. Rothenberg, Ceramic membranes: new opportunities and practical applications, John Wiley & Sons,, 2016.

[39] T. Van Gestel, D. Sebold, Hydrothermally stable mesoporous ZrO_2 membranes prepared by a facile nanoparticle deposition process, Sep. Purif. Technol. 221 (2019) 399–407, https://doi.org/10.1016/j.seppur.2019.03.066.

[40] R. Neufert, M. Moeller, A.K. Bakshi, Dead-end silicon carbide micro-filters for liquid, Filtration, (2013) 113–125, https://doi.org/10.1002/9781118807811.ch10.

[41] R.J. Ciora, B. Fayyaz, P.K.T. Liu, V. Suwanmethanond, R. Mallada, M. Sahimi, T. T. Tsotsis, Preparation and reactive applications of nanoporous silicon carbide membranes, Chem. Eng. Sci. 59 (2004) 4957–4965, https://doi.org/10.1016/j.ces.2004.07.015.

[42] M. Fraga, S. Sanches, J. Crespo, V. Pereira, Assessment of a new silicon carbide tubular honeycomb membrane for treatment of olive mill wastewaters, Membr. (Basel) 7 (2017) 12, https://doi.org/10.3390/membranes7010012.

[43] Zhongyang Li, K. Kusakabe, S. Morooka, Preparation of thermostable amorphous Si□C□O membrane and its application to gas separation at elevated temperature, J. Memb. Sci. 118 (1996) 159–168, https://doi.org/10.1016/0376-7388(96)00086-5.

[44] E. Eray, V. Boffa, M.K. Jørgensen, G. Magnacca, V.M. Candelario, Enhanced fabrication of silicon carbide membranes for wastewater treatment: from laboratory to industrial scale, J. Memb. Sci. (2020), 118080, https://doi.org/10.1016/j.memsci.2020.118080.

[45] M.A. Rahman, M. Ha, D. Othman, A.F. Ismail, Morphological study of yttria-stabilized zirconia hollow fi bre membrane prepared using phase inversion / sintering technique 41 (2015) 12543–12553, https://doi.org/10.1016/j.ceramint.2015.06.066.

[46] E. Bet-moushoul, Y. Mansourpanah, K. Farhadi, M. Tabatabaei, TiO_2 nanocomposite based polymeric membranes: A review on performance improvement for various applications in chemical engineering processes, Chem. Eng. J. 283 (2016) 29–46, https://doi.org/10.1016/j.cej.2015.06.124.

[47] U. Aust, S. Benfer, M. Dietze, A. Rost, G. Tomandl, Development of microporous ceramic membranes in the system TiO_2/ZrO_2, J. Memb. Sci. 281 (2006) 463–471, https://doi.org/10.1016/j.memsci.2006.04.016.

[48] T. Fukumoto, T. Yoshioka, H. Nagasawa, M. Kanezashi, T. Tsuru, Development and gas permeation properties of microporous amorphous TiO_2–ZrO_2–organic

composite membranes using chelating ligands, J. Memb. Sci. 461 (2014) 96–105, https://doi.org/10.1016/j.memsci.2014.02.031.
[49] G.N. Shao, S.M. Imran, S.J. Jeon, M. Engole, N. Abbas, M. Salman Haider, S. J. Kang, H.T. Kim, Sol–gel synthesis of photoactive zirconia–titania from metal salts and investigation of their photocatalytic properties in the photodegradation of methylene blue, Powder Technol. 258 (2014) 99–109, https://doi.org/10.1016/j.powtec.2014.03.024.
[50] Q. Xu, M.A. Anderson, Sol-gel route to synthesis of microporous ceramic membranes: thermal stability of TiO_2-ZrO_2 mixed oxides, J. Am. Ceram. Soc. 76 (1993) 2093–2097, https://doi.org/10.1111/j.1151-2916.1993.tb08338.x.
[51] C. Gionco, M.C. Paganini, E. Giamello, O. Sacco, V. Vaiano, D. Sannino, Rare earth oxides in zirconium dioxide: How to turn a wide band gap metal oxide into a visible light active photocatalyst, J. Energy Chem. 26 (2017) 270–276, https://doi.org/10.1016/j.jechem.2016.07.006.
[52] F. Bortot Coelho, C. Gionco, M. Paganini, P. Calza, G. Magnacca, Control of membrane fouling in organics filtration using ce-doped zirconia and visible light, Nanomaterials 9 (2019) 534, https://doi.org/10.3390/nano9040534.
[53] C. Gionco, M.C. Paganini, E. Giamello, R. Burgess, C. Di Valentin, G. Pacchioni, Cerium-doped zirconium dioxide, a visible-light-sensitive photoactive material of third generation, J. Phys. Chem. Lett. 5 (2014) 447–451, https://doi.org/10.1021/jz402731s.
[54] U. Aust, T. Moritz, U. Popp, G. Tomandl, Direct synthesis of ceramic membranes by sol-gel process, J. Sol. -Gel Sci. Technol. 26 (2003) 715–720, https://doi.org/10.1023/A:1020789903666.
[55] D. Li, H. Wang, W. Jing, Y. Fan, W. Xing, Fabrication of mesoporous TiO_2 membranes by a nanoparticle-modified polymeric sol process, J. Colloid Interface Sci. 433 (2014) 43–48, https://doi.org/10.1016/j.jcis.2014.05.026.
[56] N. Barbero, D. Vione, Why dyes should not be used to test the photocatalytic activity of semiconductor oxides, Environ. Sci. Technol. 50 (2016) 2130–2131, https://doi.org/10.1021/acs.est.6b00213.
[57] G. Witz, V. Shklover, W. Steurer, S. Bachegowda, H.P. Bossmann, Phase evolution in yttria-stabilized zirconia thermal barrier coatings studied by rietveld refinement of X-ray powder diffraction patterns, J. Am. Ceram. Soc. 90 (2007) 2935–2940, https://doi.org/10.1111/j.1551-2916.2007.01785.x.
[58] H.G. Scott, Phase relationships in the zirconia-yttria system, J. Mater. Sci. 10 (1975) 1527–1535, https://doi.org/10.1007/BF01031853.
[59] N. Veronovski, P. Andreozzi, C. La Mesa, M. Sfiligoj-Smole, Stable TiO_2 dispersions for nanocoating preparation, Surf. Coat. Technol. 204 (2010) 1445–1451, https://doi.org/10.1016/j.surfcoat.2009.09.041.
[60] S. Ciston, R.M. Lueptow, K.A. Gray, Bacterial attachment on reactive ceramic ultrafiltration membranes, J. Memb. Sci. 320 (2008) 101–107, https://doi.org/10.1016/j.memsci.2008.03.065.
[61] T. Ohno, K. Sarukawa, K. Tokieda, M. Matsumura, Morphology of a TiO_2 photocatalyst (Degussa, P-25) consisting of anatase and rutile crystalline phases, J. Catal. 203 (2001) 82–86, https://doi.org/10.1006/jcat.2001.3316.
[62] D.A.H. Hanaor, C.C. Sorrell, Review of the anatase to rutile phase transformation, J. Mater. Sci. 46 (2011) 855–874, https://doi.org/10.1007/s10853-010-5113-0.
[63] M.K. Akhtar, S.E. Pratsinis, S.V.R. Mastrangelo, Dopants in vapor-phase synthesis of titania powders, J. Am. Ceram. Soc. 75 (1992) 3408–3416, https://doi.org/10.1111/j.1151-2916.1992.tb04442.x.
[64] B. Menezes, D. Moreira, H. Oliveira, L. Marques, J. Lima, Solvothermal synthesis of cerium-doped titania nanostructured materials modified with acetylacetone for solar-driven photocatalysis, J. Braz. Chem. Soc. (2020), https://doi.org/10.21577/0103-5053.20190148.
[65] S. Hernández, C. Gionco, T. Husak, M. Castellino, J.A. Muñoz-Tabares, K.R. Tolod, E. Giamello, M.C. Paganini, N. Russo, Insights into the sunlight-driven water oxidation by Ce and Er-doped ZrO_2, Front. Chem. 6 (2018), https://doi.org/10.3389/fchem.2018.00368.
[66] F.E. Bortot Coelho, V.M. Candelario, E.M.R. Araújo, T.L.S. Miranda, G. Magnacca, Photocatalytic reduction of Cr(VI) in the presence of humic acid using immobilized Ce–ZrO_2 under visible light, Nanomaterials 10 (2020) 779, https://doi.org/10.3390/nano10040779.
[67] C. Gionco, A. Battiato, E. Vittone, M.C. Paganini, E. Giamello, Structural and spectroscopic properties of high temperature prepared ZrO_2-TiO_2 mixed oxides, J. Solid State Chem. 201 (2013) 222–228, https://doi.org/10.1016/j.jssc.2013.02.040.
[68] H.E. Garrafa-Gálvez, C.G. Alvarado-Beltrán, J.L. Almaral-Sánchez, A. Hurtado-Macías, A.M. Garzon-Fontecha, P.A. Luque, A. Castro-Beltrán, Graphene role in improved solar photocatalytic performance of TiO_2-rGO nanocomposite, Chem. Phys. 521 (2019) 35–43, https://doi.org/10.1016/j.chemphys.2019.01.013.
[69] G.D. Parfitt, Surface chemistry of oxides, Pure Appl. Chem. 48 (1976) 415–418, https://doi.org/10.1351/pac197648040415.
[70] D.L. Liao, G.S. Wu, B.Q. Liao, Zeta potential of shape-controlled TiO_2 nanoparticles with surfactants, Colloids Surf. A Physicochem. Eng. Asp. 348 (2009) 270–275, https://doi.org/10.1016/j.colsurfa.2009.07.036.
[71] M. Kosmulski, P. Próchniak, J.B. Rosenholm, Letter: the IEP of carbonate-free neodymium(III) oxide, J. Dispers. Sci. Technol. 30 (2009) 589–591, https://doi.org/10.1080/01932690902766319.
[72] S.Z.A. Bukhari, J. Ha, J. Lee, I. Song, Effect of different heat treatments on oxidation-bonded SiC membrane for water filtration, Ceram. Int. 44 (2018) 14251–14257, https://doi.org/10.1016/j.ceramint.2018.05.029.
[73] P. Boch, J.-C. Niepce. Ceramic materials: processes, properties, and applications, John Wiley & Sons,, 2010.
[74] K.B. Singh, M.S. Tirumkudulu, Cracking in drying colloidal films, Phys. Rev. Lett. 98 (2007), 218302, https://doi.org/10.1103/PhysRevLett.98.218302.
[75] M.S. Tirumkudulu, W.B. Russel, Cracking in drying latex films, Langmuir 21 (2005) 4938–4948, https://doi.org/10.1021/la048298k.
[76] M. Qiu, Y. Fan, N. Xu, Preparation of supported zirconia ultrafiltration membranes with the aid of polymeric additives, J. Memb. Sci. 348 (2010) 252–259, https://doi.org/10.1016/j.memsci.2009.11.009.
[77] K. Boussu, B. Van der Bruggen, A. Volodin, C. Van Haesendonck, J.A. Delcour, P. Van der Meeren, C. Vandecasteele, Characterization of commercial nanofiltration membranes and comparison with self-made polyethersulfone membranes, Desalination 191 (2006) 245–253, https://doi.org/10.1016/j.desal.2005.07.025.
[78] N. Saffaj, R. Mamouni, A. Laknifli, A. Mouna, S.A. Younssi, A. Albizane, Efficiency of ultrafiltration ceramic membranes for toxic elements removal from wastewaters, Sci. Study Res. Chem. Chem. Eng. 11 (2010) 243–254.
[79] N. Aryanti, A. Saraswati, R. Pratama Putra, A. Nafiunisa, D.H. Wardhani, Fouling mechanism of micelle enhanced ultrafiltration with Sds surfactant for indigozol dye removal, J. Teknol. 80 (2018) 29–36, https://doi.org/10.11113/jt.v80.12741.
[80] J. Kaewsuk, G.T. Seo, Computational study of NF membrane removal in rejection of specific NOM compounds, Desalin. Water Treat. 51 (2013) 6218–6223, https://doi.org/10.1080/19443994.2013.780788.
[81] L.F. Albuquerque, A.A. Salgueiro, J.L. de, S. Melo, O. Chiavone-Filho, Coagulation of indigo blue present in dyeing wastewater using a residual bittern, Sep. Purif. Technol. 104 (2013) 246–249, https://doi.org/10.1016/j.seppur.2012.12.005.
[82] M. Mahzoura, N. Tahri, M. Daramola, J. Duplay, G. Schäfer, R. Ben Amar, M. Mahzoura, N. Tahri, M. Daramola, J. Duplay, G. Schäfer, Comparative investigation of indigo blue dye removal efficiency of activated carbon and natural clay in adsorption/ultrafiltration system, Desalin. Water Treat. 164 (2019) 326–338.
[83] D. Shen, J. Fan, W. Zhou, B. Gao, Q. Yue, Q. Kang, Adsorption kinetics and isotherm of anionic dyes onto organo-bentonite from single and multisolute systems, J. Hazard. Mater. 172 (2009) 99–107, https://doi.org/10.1016/j.jhazmat.2009.06.139.
[84] F. de Souza, S.R. Bragança, Extraction and characterization of humic acid from coal for the application as dispersant of ceramic powders, J. Mater. Res. Technol. 7 (2018) 254–260, https://doi.org/10.1016/j.jmrt.2017.08.008.
[85] C. Li, W. Sun, Z. Lu, X. Ao, C. Yang, S. Li, Systematic evaluation of TiO_2-GO-modified ceramic membranes for water treatment: Retention properties and fouling mechanisms, Chem. Eng. J. 378 (2019), 122138, https://doi.org/10.1016/j.cej.2019.122138.
[86] G. Zhan, C. Li, D. Luo, Electrochemical investigation of bovine hemoglobin at an acetylene black paste electrode in the presence of sodium dodecyl sulfate, Bull. Korean Chem. Soc. 28 (2007) 1720–1724, https://doi.org/10.5012/bkcs.2007.28.10.1720.
[87] Z.G. Peng, K. Hidajat, M.S. Uddin, Adsorption of bovine serum albumin on nanosized magnetic particles, J. Colloid Interface Sci. 271 (2004) 277–283, https://doi.org/10.1016/j.jcis.2003.12.022.
[88] A. Larbot, J. -P. Fabre, C. Guizard, L. Cot, J. Gillot, New inorganic ultrafiltration membranes: titania and zirconia membranes, J. Am. Ceram. Soc. 72 (1989) 257–261, https://doi.org/10.1111/j.1151-2916.1989.tb06111.x.
[89] S.N. Hosseini, S.M. Borghei, M. Vossoughi, N. Taghavinia, Immobilization of TiO_2 on perlite granules for photocatalytic degradation of phenol, Appl. Catal. B Environ. 74 (2007) 53–62, https://doi.org/10.1016/j.apcatb.2006.12.015.
[90] M. Sarro, N.P. Gule, E. Laurenti, R. Gamberini, M.C. Paganini, P.E. Mallon, P. Calza, ZnO-based materials and enzymes hybrid systems as highly efficient catalysts for recalcitrant pollutants abatement, Chem. Eng. J. 334 (2018) 2530–2538, https://doi.org/10.1016/j.cej.2017.11.146.
[91] N.M. Mahmoodi, M. Arami, N.Y. Limaee, N.S. Tabrizi, Kinetics of heterogeneous photocatalytic degradation of reactive dyes in an immobilized TiO_2 photocatalytic reactor, J. Colloid Interface Sci. 295 (2006) 159–164, https://doi.org/10.1016/j.jcis.2005.08.007.
[92] A.U. Rajapaksha, M.S. Alam, N. Chen, D.S. Alessi, A.D. Igalavithana, D.C.W. Tsang, Y.S. Ok, Removal of hexavalent chromium in aqueous solutions using biochar: chemical and spectroscopic investigations, Sci. Total Environ. 625 (2018) 1567–1573, https://doi.org/10.1016/j.scitotenv.2017.12.195.
[93] J.L. Wang, L.J. Xu, Advanced oxidation processes for wastewater treatment: formation of hydroxyl radical and application, Crit. Rev. Environ. Sci. Technol. 42 (2012) 251–325, https://doi.org/10.1080/10643389.2010.507698.
[94] E. García-López, G. Marcì, F.R. Pomilla, M.C. Paganini, C. Gionco, E. Giamello, L. Palmisano, ZrO_2 based materials as photocatalysts for 2-propanol oxidation by using UV and solar light irradiation and tests for CO_2 reduction, Catal. Today 313 (2018) 100–105, https://doi.org/10.1016/j.cattod.2018.01.030.
[95] V. Diesen, M. Jonsson, Formation of H_2O_2 in TiO_2 photocatalysis of oxygenated and deoxygenated aqueous systems: a probe for photocatalytically produced hydroxyl radicals, J. Phys. Chem. C. 118 (2014) 10083–10087, https://doi.org/10.1021/jp500315u.
[96] Z. Jiang, L. Wang, J. Lei, Y. Liu, J. Zhang, Photo-fenton degradation of phenol by CdS/rGO/Fe2+ at natural pH with in situ-generated H_2O_2, Appl. Catal. B Environ. 241 (2019) 367–374, https://doi.org/10.1016/j.apcatb.2018.09.049.
[97] S. Sun, H. Yao, W. Fu, L. Hua, G. Zhang, W. Zhang, Reactive photo-fenton ceramic membranes: synthesis, characterization and antifouling performance, Water Res 144 (2018) 690–698, https://doi.org/10.1016/j.watres.2018.08.002.
[98] G. Xue, H. Liu, Q. Chen, C. Hills, M. Tyrer, F. Innocent, Synergy between surface adsorption and photocatalysis during degradation of humic acid on TiO_2/activated carbon composites, J. Hazard. Mater. 186 (2011) 765–772, https://doi.org/10.1016/j.jhazmat.2010.11.063.
[99] A. Asatekin, S. Kang, M. Elimelech, A.M. Mayes, Anti-fouling ultrafiltration membranes containing polyacrylonitrile-graft-poly(ethylene oxide) comb

copolymer additives, J. Memb. Sci. 298 (2007) 136–146, https://doi.org/10.1016/j.memsci.2007.04.011.